International Journal of Heat and Mass Transfer 156 (2020) 119792

Contents lists available at ScienceDirect

International Journal of Heat and Mass Transfer

journal homepage: www.elsevier.com/locate/hmt

Study of thermal and hydrodynamic characteristics of water-nano-encapsulated phase change particles suspension in an annulus of a porous eccentric horizontal cylinder

Mohammad Ghalambaz[a,b,*], S.A.M. Mehryan[c], Masoud Mozaffari[d], Seyed Mohsen Hashem Zadeh[e], Mohsen Saffari Pour[f,g]

[a] Metamaterials for Mechanical, Biomechanical and Multiphysical Applications Research Group, Ton Duc Thang University, Ho Chi Minh City, Vietnam
[b] Faculty of Applied Sciences, Ton Duc Thang University, Ho Chi Minh City, Vietnam
[c] Young Researchers and Elite Club, Yasooj Branch, Islamic Azad University, Yasooj, Iran
[d] Department of Mechanical Engineering, Najafabad Branch, Islamic Azad University, Najafabad, Iran
[e] Department of Mechanical Engineering, Shahid Chamran University of Ahvaz, Ahvaz, Iran
[f] Department of Mechanical Engineering, Shahid Bahonar University of Kerman, Kerman, Iran
[g] Division of Processes, KTH Royal Institute of Technology, Stockholm, Sweden

ARTICLE INFO

Article history:
Received 24 February 2020
Revised 8 April 2020
Accepted 9 April 2020
Available online 20 May 2020

Keywords:
Eccentric horizontal cylinder
Enhanced Heat Transfer
Nano Encapsulated Phase Change Material (NEPCM)
Porous media

ABSTRACT

In this paper, the thermal and hydrodynamic characteristics of a suspension with water-Nano-Encapsulated Phase Change Material (NEPCM) in an annulus of a porous eccentric horizontal cylinder are investigated. The NEPCM particles have a core-shell structure and stability suspended in water. Hence, the particles, along with the liquid, could freely circulate inside the annuli of the horizontal cylinder due to the buoyancy forces. The cores of these particles are made from a Phase Change Material (PCM). Moreover, such cores are in a continuous exchange of heat transfer between the solid and liquid phases. The heat transfer is acting in a combination of absorption, storage, and release mechanisms. The governing equations for the fluid motions and conservation of energy could be written in partial differential forms and by using the appropriate non-dimensional variables converted into non-dimensional ones. Then, the numerical approach is applied by implementing the finite element method (FEM) to solve such equations iteratively. The impact of various non-dimensional parameters including the fusion temperature, Stefan number, Rayleigh number, Darcy number, the volume fraction of nanoparticles, and eccentricity of the inner cylinder is addressed on the flow and heat transfer. It is observed that the most favourable fusion temperature ranges for the maximum heat transfer rate vary as a function of the Rayleigh number. In addition, the heat transfer rate can be enhanced by applying the phase change core of nanoparticles.

© 2020 Elsevier Ltd. All rights reserved.

1. Introduction

Nowadays, the usage of Phase Change Materials (PCMs) has been extensively reported in thermal storage applications. The ability of materials as such in storing and releasing heat attracted the attention of researchers to combine them with nano-sized particles. This combination can easily enhance the heat transfer rate dramatically, which is reported by several researchers during the past decade.

Fluid-saturated porous media due to the thermally driven flows in their porous regions could be involved in a variety of applied areas in micro/nano-engineering. The metal foams can provide a high thermal conductive structure for improvement of the heat transfer rate in enclosures and illuminate a bright future for nano-involved PCMs. The encapsulation is a method, which introduces a phase change material (PCM) into a polymeric shell or in a porous matrix. By using encapsulation, the heat can easily transfer between the phase change core and surroundings and the leakage problem will be highly eliminated. One of the novel practical application of nanofluids is the encapsulation of phase change materials in nano-sized particles. Later, the Nano-Encapsulated Phase Change Materials (NEPCMs) particles can be evenly distributed in a liquid to produce a suspension of NEPCM. The thermo-fluid properties of the

* Corresponding author.
E-mail addresses: mohammad.ghalambaz@tdtu.edu.vn (M. Ghalambaz), mohsen.hashemzadeh@gmail.com (S.M. Hashem Zadeh), mohsensp@kth.se (M. Saffari Pour).

https://doi.org/10.1016/j.ijheatmasstransfer.2020.119792
0017-9310/© 2020 Elsevier Ltd. All rights reserved.

Nomenclature

Latin symbols

C_p	Constant pressure specific heat
Cr	Suspension's heat capacity ratio
Da	Darcy number
e	Eccentricity
E_c	Dimensionless eccentricity
f	Dimensionless fusion function
g	Acceleration of gravity
H	Characteristic length for non-dimensionalization
k	Coefficient of the thermal conductivity
K	Permeability of the porous medium
L	Size of the cavity, the characteristic length
Nc	Conductivity number for NEPCM suspension
Nu	Nusselt number
Nv	Dynamic viscosity number for NEPCM suspension
R_i	Radius of inner cylinder
R_o	Radius of outer cylinder
R_r	Radii ratio
Ra	Rayleigh number
Ste	Stefan number
u	x-velocity
U	Dimensionless velocity in X-direction
v	y-velocity component
V	Dimensionless velocity in Y-direction
x	x-Cartesian coordinate
X	Dimensionless x-Cartesian coordinate
y	y-Cartesian coordinate
Y	Dimensionless y-Cartesian coordinate

Greek symbols

μ	Fluid's dynamic viscosity
α	Coefficient of thermal diffusivity
β	Thermal coefficient of thermal expansion
δ	Dimensionless melting interval
θ	Dimensionless form of the temperature field
λ	Sensible heat-capacity ratio of the Suspension
φ	Volumetric fraction of the encapsulated particles in the host fluid
ι	Weight ratio of the NEPCM-core to NEPCM-shell

Subscript

b	Bulk properties of the NEPCM-suspension
co	The core of NEPCM particle, Cold wall
fu	The phase change
h	Hot surface
p	NEPCM particles
m	Porous medium
s	Solid matrix
sh	NEPCM particle's shell

NEPCM-suspensions in a porous medium are another interesting module with lots of unknown phenomena that need enormous efforts to discover the complexity of it.

In recent years, nanofluids have been firstly introduced by prominent researchers like Choi [1], and later, their natural convection was investigated by Khanafer et al. [2]. Later on, their potential usages in electronics and engineering fields have been examined completely by numerous research activities. There are various reports regarding the present and future implementation of nanofluids published by Das et al. [3], Shenoy et al. [4], Nield and Bejan[5], and Mahian et al. [6, 7]. Moreover, excellent attempts in heat transfer enhancement of PCMs [8, 9] and nano-enhanced phase change materials [10, 11] in enclosures can be found in the literature. Various aspect of natural convection of nanofluids such as homogeneous nanofluids[12, 13], non- homogeneous nanofluids[14, 15], porous medium [16], magnetic field effects [17, 18], entropy generation [19, 20], and conjugate heat transfer effects [21] have been addressed.

The phase change materials as a mean for thermal energy storage have been received much attention in recent years. Using embedded solid fins [8, 22] in PCMs, dispersing of thermal conductive nanoparticles in PCMs [10, 23], embedding PCMs in metal foams [24, 25], or a combination of metal foams and nanoparticles [26] are several approaches to improve the bulk thermal conductivity of phase change materials. However, encapsulation of PCMs is a unique approach, which allows the phase change occurs in a liquid suspension with a large surface of heat transfer interaction between liquid and PCM.

Various types of NEPCMs have been synthesized and advanced in the past decade [27]. Some researchers focused on their thermal cycles, such as what reported in [27]. On the other hand, Zhu et al. [28] tried to enhance the thermal behaviour of the NEPCMs by using hybrid particles. According to the findings by Zhao et al. [29], it would be possible to fabricate micro-encapsulated phase change materials (MEPCMs) by means of Titania-Polyurea (TiO_2-PUA) shell. Besides, Zhu et al. [30] found that the shell of small size capsules with highly conductive metals like Ag could enhance the heat transfer rate to some extent. The core of their fabricated PCM's was made of noctacosane, which results in low fusion temperature in the vicinity of the core. Navarrete et al. [31] tried to use the special NEPCM in highly temperature-dependent solar systems. Du et al. [32] used flame retardant properties of PCMs made by n-octadecane in a shell of modified melamine–formaldehyde. In another try for the suspensions of encapsulated PCMs, Barlak et al. [27] successively analyzed the thermo-fluid properties. Their findings proved that the concentration of 3.36% of NEPCM particles could improve the fluid thermal conductivity up to 20%.

Most of the proposed worksin literature are concerned with the preparation of the NEPCMs or synthesize of their suspensions. There are a few works related to the thermal and hydrodynamic characteristics of the NEPCM-suspensions. Most of the available reports considered such characteristics in simple smooth geometries like channels/tubes. For example, a theoretical study was performed for the heat transfer improvement in microtube heat sinks by encapsulated PCMs [33], and it was concluded that the NEPCM suspension inside a host fluid could lead to an improvement of the cooling power of the system and a significant pressure drop was observed in the tube. Seyf et al. [34] numerically investigated the thermal and hydrodynamic behaviour of a nano-encapsulated octadecane slurry flows over a square cylinder. They revealed that the heat transfer rate was enhanced by using such slurry compare to the base fluid.

Ho et al. [35] experimentally investigated the effects of applying water-based micro-encapsulated PCM in a minichannel. They detected that the thermal properties could be influenced by the existence of the PCM capsules and other factors like the fluid flow rate and the heat exchange ratio. There are also experimental approaches that used various metallic nanoparticles and/or slurries of micro-encapsulated PCMs in tubes [36] and minichannels [37]. Eisapour et al. [38] employed a slurry of microencapsulated PCMs for cooling of photovoltaic cells. The results show that using the slurry can efficiently reduce the operating temperature of photovoltaic panels.

Few studies investigated the flow and heat transfer of NEPCMs in natural convective flows. Ghalambaz et al. [39] modelled the steady-state free convection heat transfer of NEPCMs in a cavity without a porous medium. Their findings indicated that using the NEPCM particles could improve heat transfer. Following Ghalambaz

Table 1
Thermo-physical properties of all involved materials in the problem [27].

	k (W/m.K)	ρ (kg/m^3)	C_p (kJ/kg.K)	μ(kg/m. s)	β(K^{-1})
Host fluid	0.613	997.1	4179	8.9×10^{-4}	21×10^{-5}
PU	–	786	1317.7	–	17.28×10^{-5}
Nonadecane	–	721	2037	–	–
Glass balls	1.05	2700	840	–	9×10^{-6}

et al. [39], Mehryan et al. [40] examined the flow and heat transfer of the NEPCM-suspensions in an eccentric annulus enclosure and found that the fusion temperature of the NEPCM particles is an essential parameter on the thermal benefit of NEPCM-suspensions. The transient phase change behaviour of the NEPCMs was also addressed in Hajjar et al. [41] in a square cavity, and the outcomes showed that the latent heat of nanoparticles could promote the heat transfer rate.

Considering the flow and heat transfer of the NEPCMs in a porous medium, the literature review shows that there are only a few studies, which investigated the convection heat transfer of the NEPCMs-suspensions in a porous medium. Ghalambaz et al. [42] investigated the boundary layer mixed convection of the NEPCM-suspensions over a flat plate embedded in a porous medium. The impacts of variations in the latent heat of nanoparticles were illustrated by the Stefan number. Moreover, in their results, the diffusive temperatures were addressed on the total heat transfer from the plate. It was found that the existence of the NEPCM particles contributes to the improvement of the heat transfer rate, and there was an optimum range of diffusive temperature to maximize the heat transfer rate. Very recently, the unsteady free convection heat transfer of NEPCMs in a square cavity filled with glass balls was investigated by Ghalambaz et al. [43]. The hot wall of the cavity was subject to periodic temperature fluctuations while the cold wall was isothermal. The results showed that using NEPCM particles could promote the heat transfer rate. The increase in the porosity could improve the heat transfer rate when the concentration of NEPCM particles was high (3%>).

As seen, the free convection heat transfer of NEPCMs-suspension in a porous medium is a new topic with a scares number of investigations. The present study aims to address the flow and heat transfer of NEPCMs in an eccentric porous cavity for the first time.

2. Physics and model formulation

The considered geometry is a porous annulus of horizontal cylinders with the inner and outer radii of r_i and r_o, respectively. As specified in Fig. 1, the inner cylinder, placed at (0, e), is maintained at the hot temperature of T_h, which is higher than the temperature of the outer cylinder T_c. The pores of the porous annulus are occupied by a suspension of water-NEPCM. The shell and core of the nano-encapsulated phase change material are made of polyurethane (PU) and nonadecane, respectively. No-slip condition for thermal and fluid behaviours exists between the liquid and the particles. Hence, the particles are uniformly dispersed in the base fluid. Moreover, zero heat flux exchange is assumed at the interface of the solid lattice and the liquid inside the porous medium. Indeed, these two structures are considered to be in a thermal equilibrium condition. The thermo-physical properties with their corresponding values for all involved materials are listed in Table 1. In addition, the fusion temperature and the latent heat for the NEPCMs core are considered to be about 32°C and 211 kJ/kg, respectively [27].

2.1. The formulation of the problem

Considering the above-mentioned assumptions, the mathematical equations for the thermal and hydrodynamic behaviour of a suspension inside a porous region have been listed below [39, 43]:

Conservation of mass:

$$\frac{\partial u}{\partial x}+\frac{\partial v}{\partial y}=0 \tag{1}$$

Conservation of momentum:

$$\frac{\rho_b}{\varepsilon^2}\left(u\frac{\partial u}{\partial x}+v\frac{\partial u}{\partial y}\right)=-\frac{\partial p}{\partial x}+\frac{\mu_b}{\varepsilon}\left(\frac{\partial^2 u}{\partial x^2}+\frac{\partial^2 u}{\partial y^2}\right)-\frac{\mu_b}{K}u \tag{2}$$

$$\frac{\rho_b}{\varepsilon^2}\left(u\frac{\partial v}{\partial x}+v\frac{\partial v}{\partial y}\right)=-\frac{\partial p}{\partial y}+\frac{\mu_b}{\varepsilon}\left(\frac{\partial^2 v}{\partial x^2}+\frac{\partial^2 v}{\partial y^2}\right)+g\rho_b\beta_b(T-T_c)-\frac{\mu_b}{K}v \tag{3}$$

Conservation of energy:

$$(\rho C_p)_b\left(u\frac{\partial T}{\partial x}+v\frac{\partial T}{\partial y}\right)=k_{m,b}\left(\frac{\partial^2 T}{\partial x^2}+\frac{\partial^2 T}{\partial y^2}\right) \tag{4}$$

where

$$k_{m,b}=(1-\varepsilon)k_s+\varepsilon k_b \tag{5}$$

The subscripts of s, m, and b in the governing equations denote the solid matrix, porous medium, and bulk properties of the NEPCM-suspension, respectively. Following the physical diagram of the enclosure, shown in Fig. 1, the boundary conditions are presented as

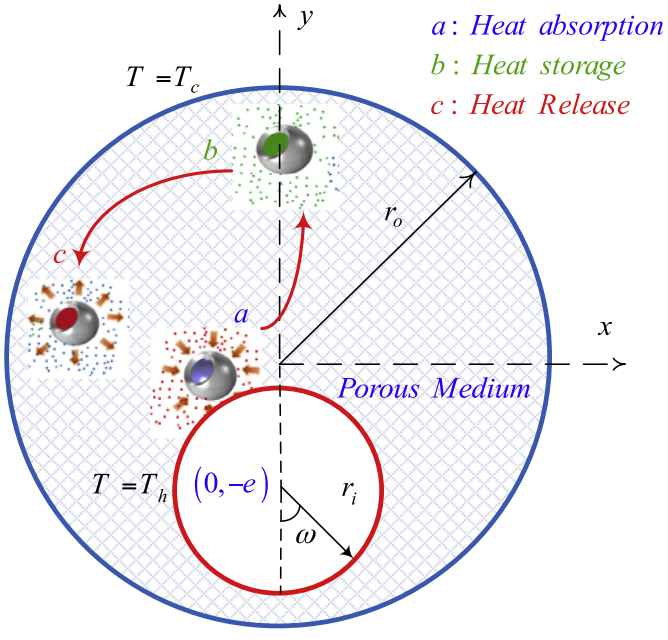

Fig. 1. Schematic configuration of the problem physics.

the following form:

$$\begin{aligned} &\forall\ x,y\left|x^2+y^2=r_o^2\ \Rightarrow u=v=0,\ T=T_c\right. \\ &\forall\ x,y\left|x^2+(y-e)^2=r_i^2\ \Rightarrow u=v=0,\ T=T_h\right. \end{aligned} \tag{6}$$

2.2. NEPCM-suspension bulk thermophysical properties

By assuming the weighted function according to the density of the host fluid and the NEPCM dispersed particles, the density of the suspension can be written as [44]:

$$\rho_b=(1-\varphi)\rho_f+\varphi\rho_p \tag{7}$$

The subscripts of f and p and indicates the base liquid and the particles, respectively. The following equation is employed to compute the NEPCM particle's density [44]:

$$\rho_p=\frac{(1+\iota)\rho_{co}\rho_{sh}}{\rho_{sh}+\iota\rho_{co}} \tag{8}$$

In the density correlated equation Eq. (8), the ρ_{sh} and ρ_{co} are the denoted densities of the shell and the core of the NEPCM particles. In this equation, ι is the core-shell weight ratio, which is taken as ι~0.447 [27]. Moreover, to the prior information, an average of the solid and liquid densities is adopted as the density of the core. The following relation is employed to compute the heat capacity of the suspension [39, 45, 46]:

$$C_{p,b}=\frac{(1-\varphi)\rho_f C_{p,f}+\varphi\rho_p C_{p,p}}{\rho_b} \tag{9}$$

For the specific heat capacity with no phase change, $C_{p,\,p,\,eff}$ is equal to the sensible heat capacity of the NEPCMs particles, i.e. $C_{p,\,p}$, which is:

$$C_{p,p}=\frac{\left(C_{p,co}+\iota C_{p,sh}\right)\rho_{co}\rho_{sh}}{(\rho_{sh}+\iota\rho_{co})\rho_p} \tag{10}$$

In the above-mentioned and all equations consisting the specific heat capacity, the average heat capacity of the fluid and solid is assumed for the core of the encapsulated nanoparticles. As the phase change material exists in the core of nanoparticles, the latent heat of such material is evaluated for the specific heat capacity calculations. The total specific heat capacity at the core of nanoparticles, which includes both sensible and latent heats is [33, 39, 44]:

$$\begin{aligned} C_{p,p,eff}&=C_{p,p}+\left\{\frac{\pi}{2}\cdot\left(\frac{h_{sf}}{T_{Mr}}-C_{p,p}\right)\cdot\sin\left(\pi\frac{T-T_{fu}+T_{Mr}/2}{T_{Mr}}\right)\right\}\gamma \\ \gamma&=\begin{cases}0 & T<T_{fu}-T_{Mr}/2\\ 1 & T_{fu}-T_{Mr}/2<T<T_{fu}+T_{Mr}/2\\ 0 & T>T_{fu}+T_{Mr}/2\end{cases} \end{aligned} \tag{11}$$

T_{Mr} denotes the temperature interval. Accordingly, such definition creates a continuous interval in the energy balance equation. The expansion coefficient due to the thermal volume changes in the suspension is prescribed as [45]:

$$\beta_b=(1-\varphi)\beta_f+\varphi\beta_p \tag{12}$$

The linear relations to evaluate the thermal conductivity and the dynamic viscosity of the suspension consisting of the fluid and nano-encapsulated particles is presented as below [23, 41, 47]:

$$\frac{k_b}{k_f}=1+Nc\,\varphi \tag{13}$$

$$\frac{\mu_b}{\mu_f}=1+Nv\,\varphi \tag{14}$$

Nc and Nv of inside the Eqs. (16) and (17) show the numbers of thermal conductivity and the number of dynamic viscosity. These values (Nc and Nv) are a function of various parameters such as type of particles, temperature, type of the base fluid, and the synthesizing method. However, these numbers could be assumed constant for a synthesized NEPCM-suspension. A linear curve-fitting on the experimental data can obtain Nc and Nv values. The important caution for using the above-presented equations is that all relations are just valid for the diluted nanofluids, i.e., $\varphi\le 0.5\%$.

2.3. Governing equations in non-dimensional form

To create dimensionless numbers, the equations describing the natural convection flow of the suspension as well as the corresponding boundary conditions, the following dimensionless parameters are employed:

$$\begin{aligned} &X=\frac{x}{H},\ Y=\frac{y}{H},\ R_i=\frac{r_i}{H},\ R_o=\frac{r_o}{H},\ E_c=\frac{e}{H},\ U=\frac{uH}{\alpha_f},\ V=\frac{vH}{\alpha_f} \\ &P=\frac{pH^2}{\rho_f\alpha_f^2},\ \theta=\frac{T-T_c}{\Delta T}. \end{aligned} \tag{15}$$

and R_r denotes the radii ratio, i.e. $r_\circ/r_i$. The length scale and the temperature scale are defined as $\Delta T=T_h-T_c, H=r_\circ-r_i$. Here, invoking the non-dimensional parameters, the dimensionless form of the governing equations along with the corresponding boundary conditions is obtained as:

$$\frac{\partial U}{\partial X}+\frac{\partial V}{\partial Y}=0 \tag{16}$$

$$\varepsilon^{-2}\left(\frac{\rho_b}{\rho_f}\right)\left(U\frac{\partial U}{\partial X}+V\frac{\partial U}{\partial Y}\right)=-\frac{\partial P}{\partial X}+Pr\varepsilon^{-1}\left(\frac{\mu_b}{\mu_f}\right)\left(\frac{\partial^2 U}{\partial X^2}+\frac{\partial^2 U}{\partial Y^2}\right)-\frac{Pr}{Da}\left(\frac{\mu_b}{\mu_f}\right)u \tag{17}$$

$$\varepsilon^{-2}\left(\frac{\rho_b}{\rho_f}\right)\left(U\frac{\partial V}{\partial X}+V\frac{\partial V}{\partial Y}\right)=-\frac{\partial P}{\partial Y}+Pr\varepsilon^{-1}\left(\frac{\mu_b}{\mu_f}\right)\left(\frac{\partial^2 V}{\partial X^2}+\frac{\partial^2 V}{\partial Y^2}\right)+Ra\cdot Pr\left(\frac{\beta_b}{\beta_f}\right)\theta-\frac{Pr}{Da}\left(\frac{\mu_b}{\mu_f}\right)v \tag{18}$$

where, the Rayleigh number, Prandtl number, and Darcy number are:

$$Ra=\frac{g\rho_f\beta_f\Delta TH^3}{\alpha_f\mu_f},\ Pr=\frac{\mu_f}{\rho_f\alpha_f},\ Da=\frac{K}{H^2} \tag{19}$$

Also,

$$\left(\frac{\rho_b}{\rho_f}\right)=(1-\varphi)+\varphi\left(\frac{\rho_p}{\rho_f}\right),\ \left(\frac{\beta_b}{\beta_f}\right)=(1-\varphi)+\varphi\left(\frac{\beta_p}{\beta_f}\right) \tag{20}$$

The thermal expansion of the particles is assumed to be very similar to the base fluid, and hence, β_b/β_f~1.

$$Cr\left(U\frac{\partial\theta}{\partial X}+V\frac{\partial\theta}{\partial Y}\right)=\left(\frac{k_{m,b}}{k_f}\right)\left(\frac{\partial^2\theta}{\partial X^2}+\frac{\partial^2\theta}{\partial Y^2}\right) \tag{21}$$

where

$$Cr=\frac{(\rho C_p)_b}{(\rho C_p)_f}=(1-\varphi)+\varphi\lambda+\frac{\varphi}{\delta\,Ste}f \tag{22}$$

$$\frac{k_{m,b}}{k_f}=(1-\varepsilon)\frac{k_s}{k_f}+\varepsilon(1+Nc\varphi) \tag{23}$$

In Eq. (22), Cr denotes the ratio of the suspension's heat capacity to the base fluid's sensible heat capacity. Besides, the sensible heat-capacity ratio (λ), the dimensionless melting interval(δ), as well as

the Stefan number (*Ste*) can be defined as follows:

$$\lambda = \frac{\left(C_{p,co} + \iota C_{p,sh}\right)\rho_{co}\rho_{sh}}{(\rho C_p)_f(\rho_{sh} + \iota\rho_{co})}, \delta = \frac{T_{Mr}}{\Delta T}, Ste = \frac{(\rho C_p)_f \Delta T(\rho_{sh} + \iota\rho_{co})}{h_{sf}\rho_{co}\rho_{sh}} \tag{24}$$

Furthermore, f, the non-dimensional fusion function, is determined as:

$$f = \frac{\pi}{2}\sin\left(\frac{\pi}{\delta}\left(\theta - \theta_{fu} + \delta/2\right)\right)\sigma$$

$$\sigma = \begin{cases} 0 & \theta < \theta_{fu} - \delta/2 \\ 1 & \theta_{fu} - \dfrac{\delta}{2} < \theta < \theta_{fu} + \delta/2 \\ 0 & \theta > \theta_{fu} + \delta/2 \end{cases} \tag{25}$$

Here, θ_{fu}, the dimensionless fusion temperature, is:

$$\theta_{fu} = \frac{T_{fu} - T_c}{\Delta T} \tag{26}$$

Eventually, the non-dimensional form of the boundary conditions is achieved:

$$\forall\, X, Y \left| X^2 + (Y - E_c)^2 = R_i^2 \right. \Rightarrow U = V = 0,\ \theta = 1 \tag{27}$$

$$\forall\, X, Y \left| X^2 + Y^2 = R_o^2 \right. \Rightarrow U = V = 0,\ \theta = 0 \tag{28}$$

Following the energy balance equation, the amount of the heat, which passes through the hot wall is equal to the amount of the energy which reaches to the NEPCM-suspension and the porous matrix, which can be obtained as:

$$Nu_l = -\left[(1-\varepsilon)\frac{k_s}{k_f} + \varepsilon(1 + Nc\,\varphi)\right]\left(\frac{\partial\theta}{\partial n}\right)_{C_i} \tag{29}$$

The integration of the local Nusselt number along the length of the heated wall gives the total heat transfer rate:

$$Nu_a = \frac{1}{2\pi}\int_0^{2\pi} Nu_l d\omega \tag{30}$$

The effect of dispersing the phase change particles in the liquid host is explored through the normalized average Nusselt numbers:

$$Nu_r' = \frac{Nu_a|_{\varphi, Ste\to\infty}}{Nu_a|_{\varphi=0}}, Nu_r'' = \frac{Nu_a|_{\varphi}}{Nu_a|_{\varphi, Ste\to\infty}} \tag{31}$$

The averaged Nusselt number of the cavity filled with porous medium and the pure liquid fluid is denoted by $Nu_a|_{\varphi=0}$. Here, Nu_r' shows the sole effect of nanoparticles on the heat transfer rate compared to the pure base-fluid. Indeed, in computing theNu_r', the Stefan number is assumed to be a very large number, which eliminates the effect of core phase change of NEPCM particles, and the sole effect of NEPCM particles would be in the change of density, thermal conductivity, and dynamic viscosity of the suspension. Likewise, the impact of the phase change core on the Nu_a is investigated byNu_r''Indeed, the infinity value for the Stefan number results in the zero value for the latent heat and the phase change role in the heat transfer rate is eliminated.

To visualize the suspension flow, observation of the streamline is essential. This can be accomplished by resolving the corresponding Poisson equation:

$$\frac{\partial^2\Psi}{\partial X^2} + \frac{\partial^2\Psi}{\partial Y^2} = -\left(\frac{\partial V}{\partial X} - \frac{\partial U}{\partial Y}\right) \tag{32}$$

along with the boundary condition of $\Psi = 0$.

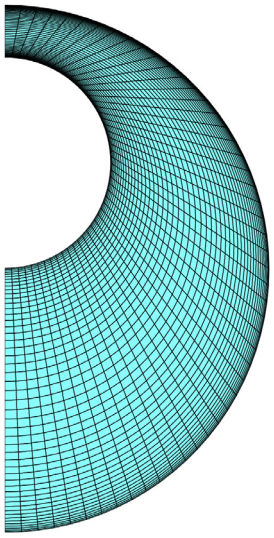

Fig. 2. Outlook of a sample of the created grid with a coase size of 25×50 for demonstration pourpose.

Table 2
Indecency of the network of grids ($Ra = 10^6$, $\theta_{fu} = 0.3$, $\varphi = 0.05$, $Pr = 6.2$, $Ste = 0.2$, $Da = 10^{-4}$, $\varepsilon = 0.9$, $E_c = 0.67$, R_r= 2.5, $\delta = 0.05$, $Nc = 23.8$, and $Nv = 12.5$).

Grid size	50×100	100×130	100×150	150×200	200×250	250×300
Nu_a	5.5059	5.5052	5.5053	5.5052	5.5051	5.5051

3. Numerical approach, grid test, and validation

In order to implement the numerical solution, a discretization is developed by adopting the Galerkin finite element method (FEM). The studied grid is formed as a non-uniform lattice. A sample of the non-uniform structured mesh with a size of 25×50 is depicted in Fig. 2.

The damped Newton method is applied to create a fully coupled system of the governing equations. Then, the problem is numerically simulated using the Parallel Sparse Direct Solver. Computations processes are done when the residuals are less than 10^{-5}. To investigate the independence of the solution procedure from the number of the grid networks, the obtained results, which including average Nusselt numbers (Nu_a) at the hot wall, are compared in Table 2. Six various non-uniform grid sizes are selected for such evaluation. Due to the small difference between the results, the network grids of 100×130 is applied for further calculation.

To verify the developed code in this study, free convection problems in two clear different horizontal cylinders occupied with air and nanofluid is tested. Fig. 3 shows the temperature fields of the work of Kuehn and Goldstein [48] and present work. The selected non-dimensional parameters in this test are $Ra = 4.7\times10^4$ and $Pr = 0.706$. Fig. 4 illustrates the average Nusselt numbers of the free convection of the nanofluid flowing in an eccentric annulus for different values of the volume fractions of the copper nanoparticles [49]. The non-dimensional parameters in this test are $Ra = 10^5$, $Pr = 6.2$, $E_c = 0.5$, and $R_r = 2.5$. In another verification, the natural convection problem in a square porous enclosed medium is analyzed. Table 3 shows the comparison of the heat transfer rates of the work of Nithiarasu et al. [50] and that of our study. As Figs. 3 and 4, and Table 3 show, the developed code in this study is accurate and dependable.

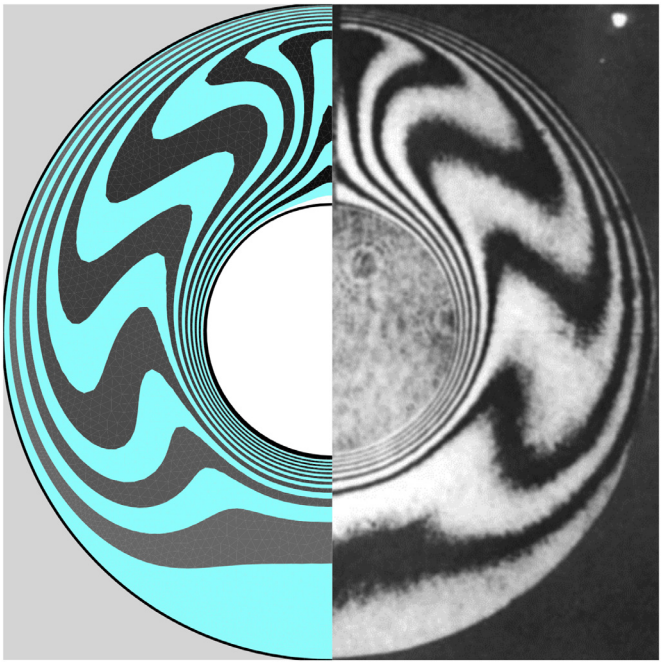

Fig. 3. Temperature fields of the present work (left side) and that of Kuehn and Goldstein [48] (right side).

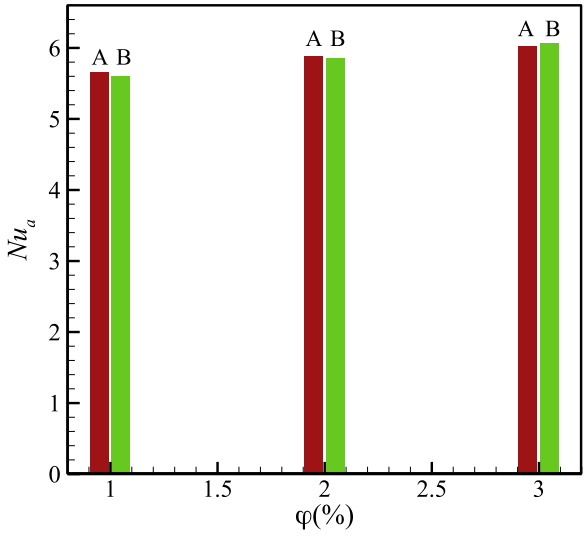

Fig. 4. The average Nusselt number resulted from the work of A: Habibi and pop [49] and B: the current study.

4. Results and discussion

This study deals with the thermal and hydrodynamic characteristics of a suspension of water and the NEPCM particles inside a porous annulus of a horizontal cylinder. According to the experimental data presented by Barlak et al. [27], the thermal conductivity *Nc* and the dynamic viscosity *Nv* numbers of the chosen suspension are 23.8 and 12.5. Besides, based on the same data, the heat capacity ratio, i.e., λ, is 0.32. The simulations are done numerically to investigate the alterable parameters including Rayleigh number ($10^4 \le Ra \le 10^6$), Stefan number ($0.2 \le Ste \le \infty$), dimensionless fusion temperature ($0.05 \le \theta_{fu} \le 1$), and the volume fraction of the particles ($0.0 \le \varphi \le 5\%$), Radii ratio ($1.67 \le R_r \le 2.5$), eccentricity ($-0.67 \le E_c \le 0.67$), Darcy number ($10^{-3} \le Da \le 10^{-1}$), and porosity ($0.3 \le \varepsilon \le 0.9$). The result section is organized in two sub-sections; first, the impact of the mentioned parameters on the outlines of the fluid and thermal fields are discussed. In the second part, the effects of the prior parameters on the heat transfer enhancement are analyzed.

Table 3
The average Nusselt number calculated in the present study and that of [50].

$Da \times Ra$	ε	Present work	Ref. [50]
10	0.4	1.078	1.078
10	0.9	1.078	1.080
10^2	0.4	1.360	1.408
10^2	0.9	1.630	1.640
10^3	0.4	7.770	7.810
10^3	0.9	9.322	9.202

4.1. Analysis of fluid flow and thermal field

Fig. 5 depicts the impact of the Rayleigh number and the eccentricity ratio on the streamlines, isolines of the temperature and the phase transition zone of the nano-sized capsules containing the nonadecane as the phase change material. It is worth noting that according to the considered model, the absorbed/released latent heat of the phase change process of the capsules is mirrored as a surge in the local value of the heat capacity of the suspension. This means that the resulting heat capacity of the suspension is, in fact, temperature-dependent.

Phase conversion of the nano-capsules occurs when their core approaches the fusion temperature, and thus, a red ribbon in the contours of the phase transition zone is formed around the corresponding nanofluid isotherm. In addition, the ribbons indicate the location of capsules that their cores are partially melted. As seen, the value of heat capacity in blue regions equals 0.97, and the PCM in the core of capsules in these areas are either entirely melted (the region around the inner hot cylinder) or solidified (the area near the cold outer cylinder).

The mechanisms of the absorption, storage, and release of the heat in the capsules can be described as follows: As a result of the exerted buoyancy volume force, two vortices, one clockwise and one counter-clockwise, are formed in the annulus. Due to the symmetry of the studied geometry, only the right half of the annulus is presented and analyzed. The flow of the suspension is upward near the hot cylinder, and it flows down in the locality of the cold one. The capsules containing phase change materials absorb energy, in the form of latent heat, while they are passing through the red ribbon of the phase transition region. As mentioned, the PCMs cores are partially melted in this region. The absorbed heat will be stored in the capsules when the temperature of the suspension is higher than their fusion temperature, i.e., throughout the blue region of *Cr* contour, around the hot cylinder, in which, the PCM in the capsules are entirely melted. The nano-capsules release their stored heat near the cold cylinder and when flowing downwardly. In other words, both mechanisms of absorption and release of the latent heat of the PCMs occur in the red region of the phase transition zone and can be identified and distinguished according to the direction of the flow.

Increasing the Rayleigh number intensifies the buoyancy force, which boosts the vortex strength. In addition, the centre of the formed vertex moves toward the narrow gap of the annulus as a result of the higher buoyant force (For $E_c = 0.67$). The isolines of the temperature are considerably distorted with the increment of the *Ra* characterizing the intensification of the convection mode of heat transfer. In addition, for $Ra = 10^6$, two more weak vortices, one in each half, are formed, circulating in the opposite direction with respect to the main vortex of each half.

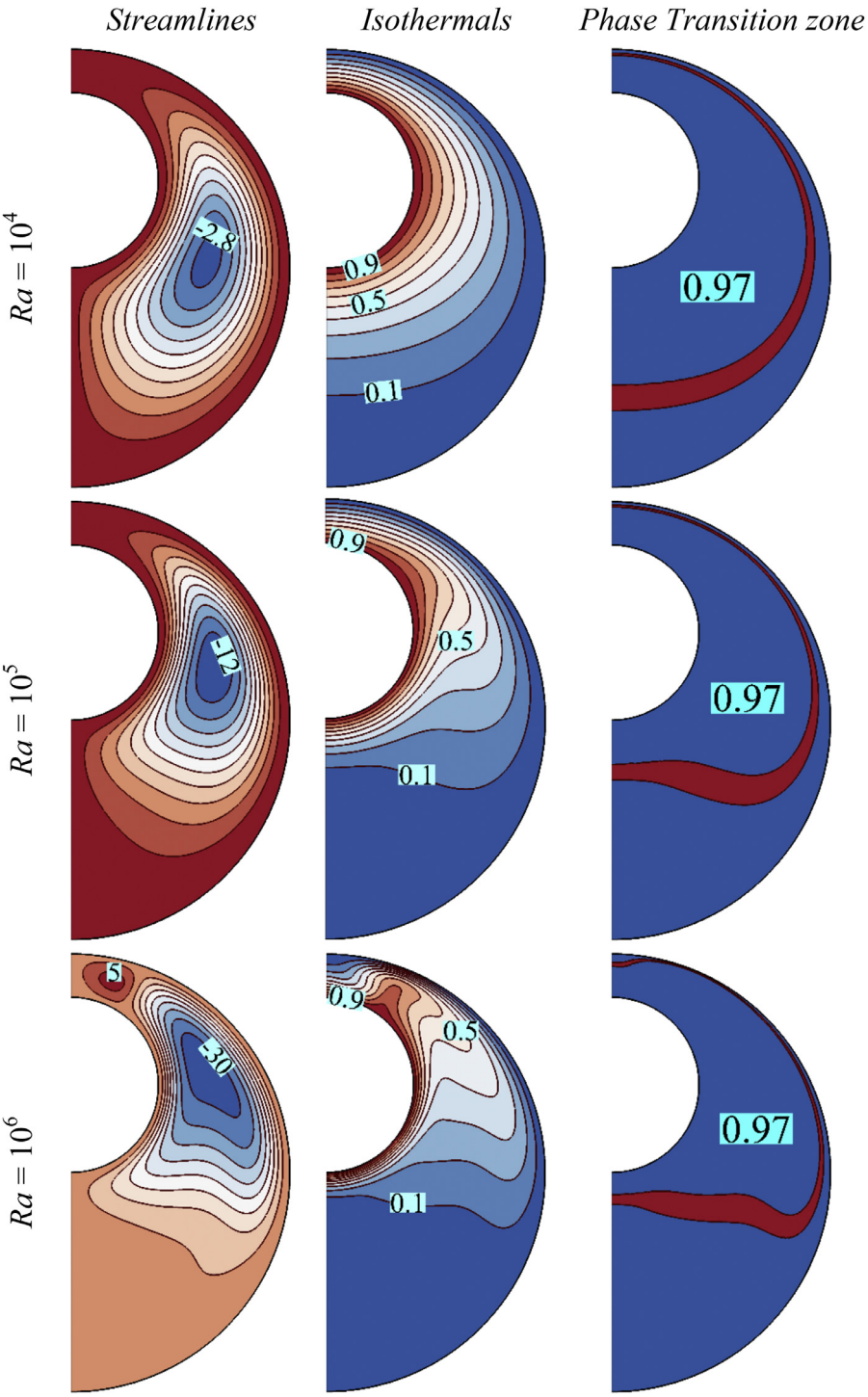

Fig. 5. Effect of the Rayleigh number on the streamlines, temperature field, and *Cr* patterns ($\theta_{fu} = 0.1$, $\varphi = 0.03$, $Da = 0.01$, $\varepsilon = Ste = 0.3$, $E_c = 0.67$ and $R_r = 2.5$).

Fig. 6 depicts the effect of the radii ratio (r_o/r_i) on the streamlines, isotherm contours, and the patterns of the phase transition zone. It should be noted that as the characteristic length for the non-dimensionalization ($H = r_o - r_i$), is considered to be identical to 1 in all simulations. As a result, a set of two linear equations is solved for each radii ratio to obtain the radius of the inner and outer cylinders. For example, for $R_r = 2.5$, $R_o$obtained as 5/3 and $R_i = 2/3$. This means that, by increasing the R_r, both radii of inner and outer cylinders will be decreased. As seen, the fluid flow enhances and distortion of the isotherms increases with decreasing the R_r. This can be explained by the fact that by reducing the radii ratio, the fluid is exposed to a larger surface area of the hot wall and thus the rate of heat transfer increases, resulting in augmentation of the fluid flow.

The influence of the location of the inner cylinder (eccentricity) on the streamlines, isotherm contours, and the patterns of the phase transition zone is illustrated in Fig. 7. The contours of streamlines reveal that the fluid flow enhances with the decline of the eccentricity. Reducing the E_c moves the hot cylinder to the region with lower average temperature, and thus, the buoyancy force

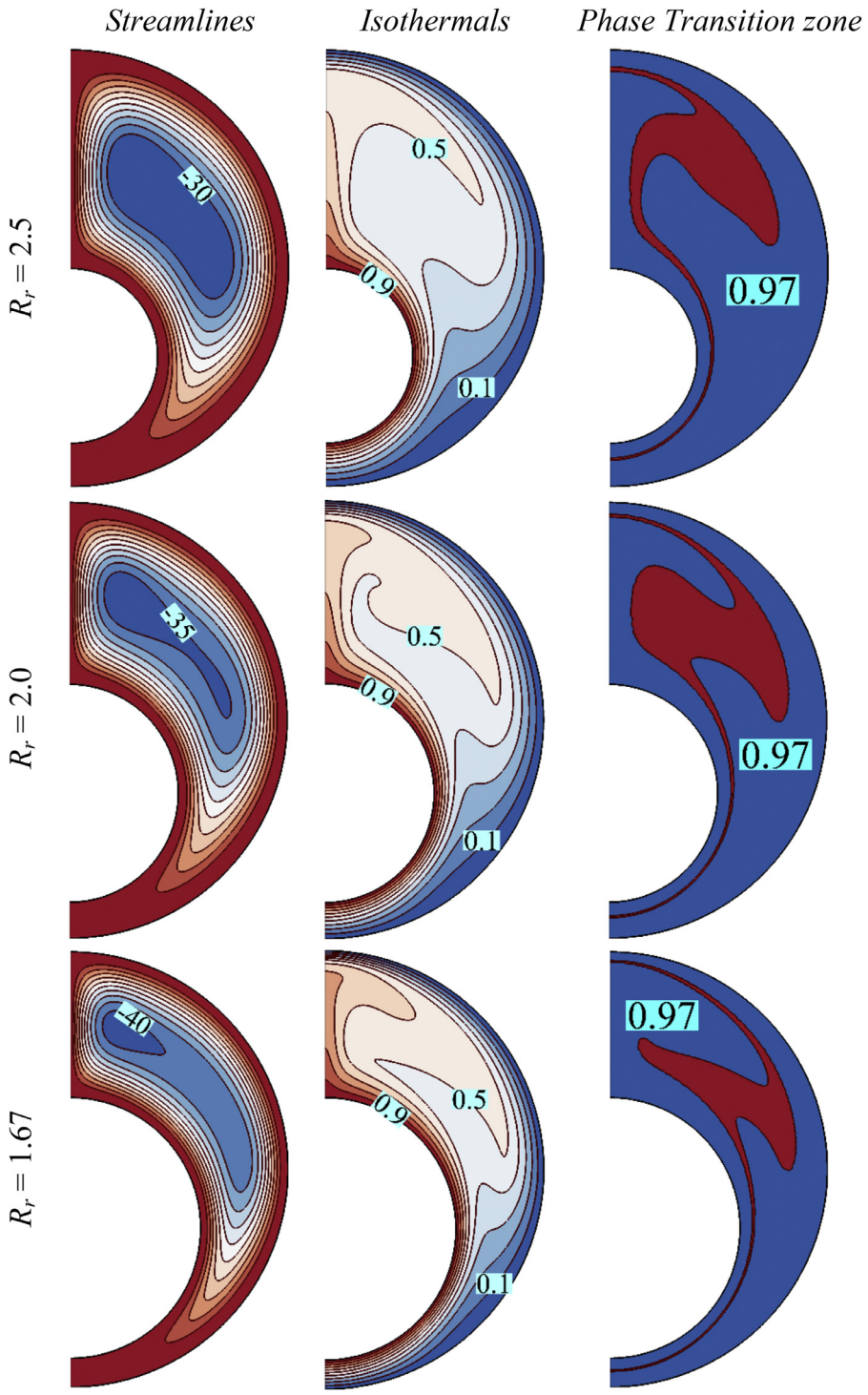

Fig. 6. Effect of the radii ratio on the streamlines, temperature field, and *Cr* patterns ($\theta_{fu} = 0.5$, $\varphi = 0.05$, $Ra = 10^5$, $Da = 0.1$, $\varepsilon = 0.6$, $Ste = 0.3$ and E_c = -0.67).

and the strength of the formed vortex intensifies. As a result, the average temperature of the cavity increases (compare isotherms of $\theta = 0.1$) and the rate of heat transfer intensifies. Moreover, the distortion of the isotherms increases with the decrease of the Eccentricity. Besides, the phase change zone enlarges as the E_c decreases, specifying that the phase transition takes place in the broader space and more capsules.

The impact of the Darcy number on the flow and thermal fields of the nanofluid is analyzed and presented in Fig. 8. Obviously, the Darcy number characterizes the permeability of the solid matrix and thus the fluid flow considerably augments as it increases. Besides, for low values of the Darcy number, the isotherms are almost vertical, indicating that the conduction is dominating mechanism in the transferred heat. By increasing the permeability on the solid matrix, the distortion of the isotherms increases. Additionally, the isothermal lines slightly move to the inner cylinder, showing the enhancement of the advection mode of heat transfer. Therefore, the phase transition zone moves toward the inner cylinder slightly. The *Cr* contours also show that the phase transition takes place in a comparatively small region. This is attributed to the high

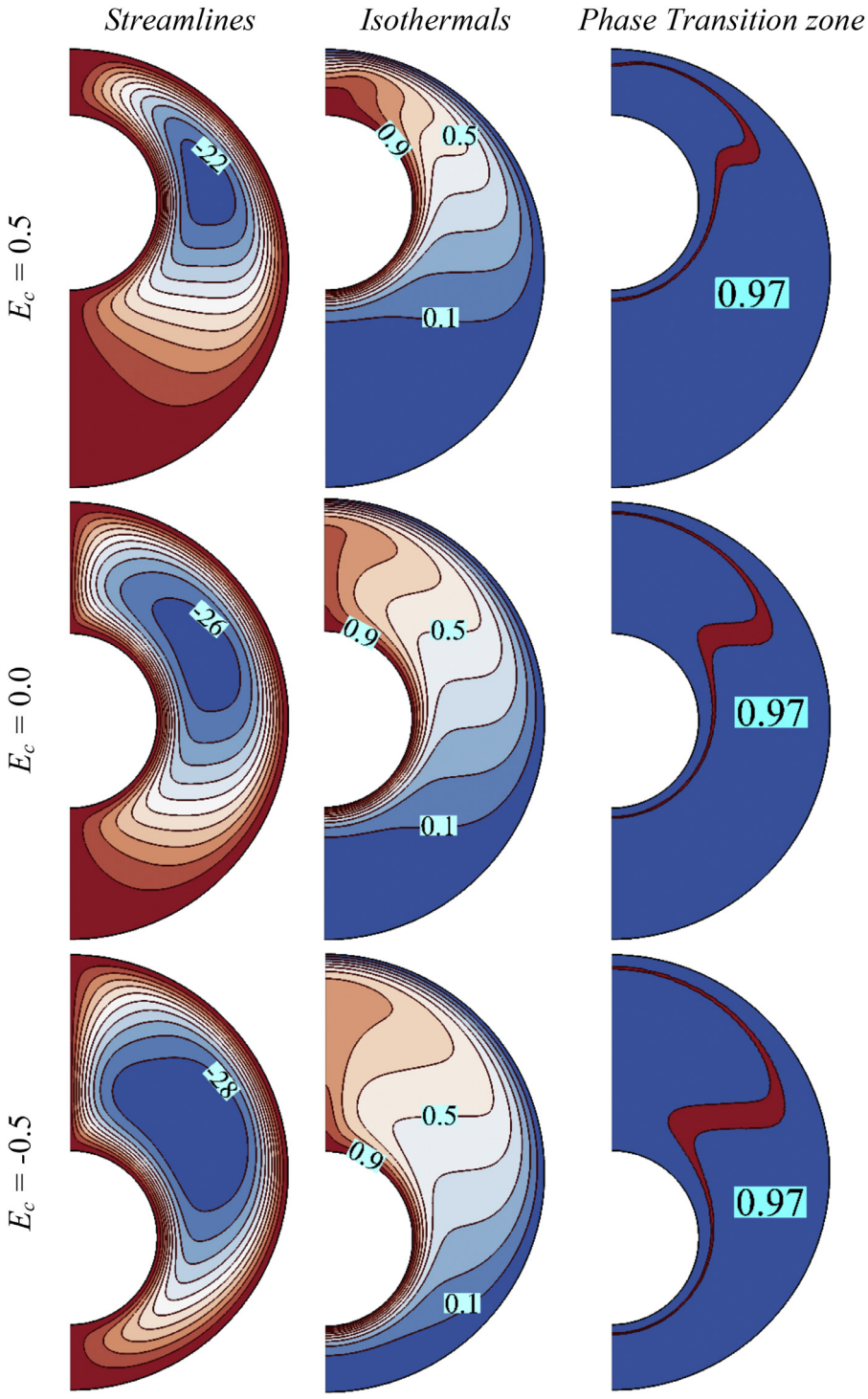

Fig. 7. Effect of the eccentricity on the streamlines, isotherm contours, and the patterns of the phase transition zone ($\theta_{fu} = 0.5$, $\varphi = 0.01$, $Ra = 10^6$, $Da = 10^{-3}$, $\varepsilon = Ste = 0.3$ and $R_r = 2.5$).

fusion temperature of the nano-capsulated PCM. In another meaning, the involvement of the capsules in the absorbing/releasing of the heat is poor. When $\theta_{fu} = 0.8$ (also same for low values of the fusion temperature), the PCMs in the capsules are in the state of solid (or liquid, when θ_{fu} is low) in almost entire of the annulus, specifying that the nano-capsules do not appropriately engage in the discussed mechanisms of absorbing/releasing heat.

To elaborate on the effect of the fusion temperature, the first row of Fig. 6 could be compared with the last row of Fig. 8, in which all of the studied parameters are the same, except the non-dimensional fusion temperature. It illustrates that when the $\theta_{fu} = 0.5$, the phase transition zone is much larger in comparison with the case of Fig. 8, showing that the phase change and the absorbing and releasing of the latent heat of the PCM are more effective than the other case. In comparison with the case of $\theta_{fu} = 0.8$, the fluid flow decreases when the fusion temperature equals 0.5. This can be explained by the fact that the temperature of the suspension remains almost constant within the phase transition zone,

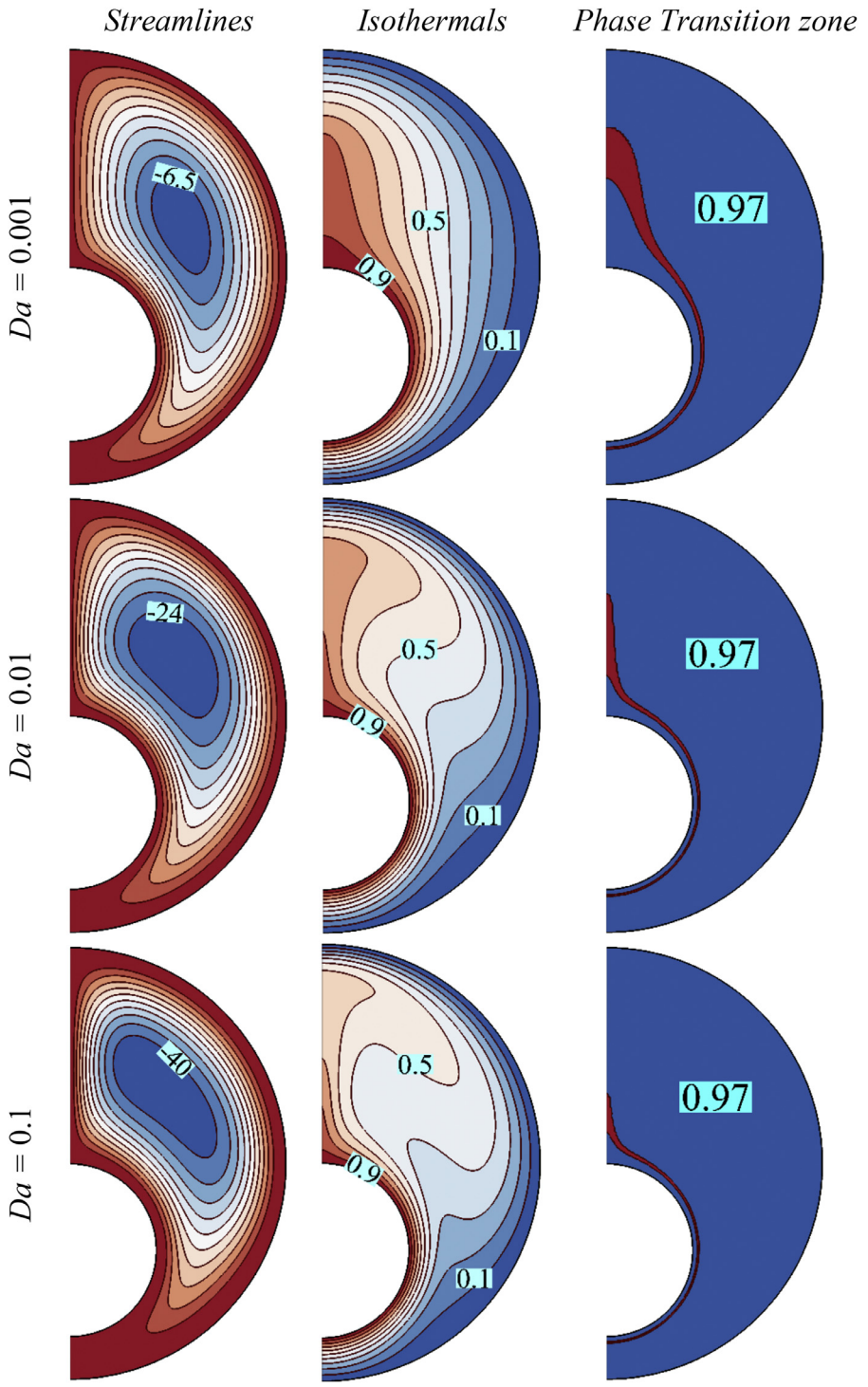

Fig. 8. Effect of the Darcy number on the streamlines, isotherm contours, and the patterns of the phase transition zone (θ_{fu} = 0.8, φ = 0.05, Ra = 10^5, ε = 0.6, Ste = 0.3, E_c = -0.67 and R_r= 2.5).

and thus the buoyancy force decreases, resulting in the reduction of fluid flow. The influence of the fusion temperature on the rate of heat transfer will be discussed in detail in Section 4.2.

4.2. Rate of heat transfer

The effects of the non-dimensional fusion temperature and the nanoparticles' volume fraction on the average Nusselt number are outlined in Fig. 9, for two values of low and high Rayleigh numbers. As seen, the rate of heat transfer intensifies with the presence of the NEPCM as it increases the average heat capacity of the suspension. Obviously, the average Nusselt number intensifies with the increment of the Rayleigh number. Moreover, for low values of the Rayleigh number, the rate of heat transfer approaches its maximum when the fusion temperature of the capsules is about 0.5, while for Ra = 10^6, the highest rate of heat transfer can be achieved when the fusion temperature differs the bond of $0.25 \leq \theta_{fu} \leq 0.65$.This specifies that the rate of heat transfer is maximum when both of the absorbing and releasing mechanisms of the latent heat of the PCM contribute appropriately. The local peaks at

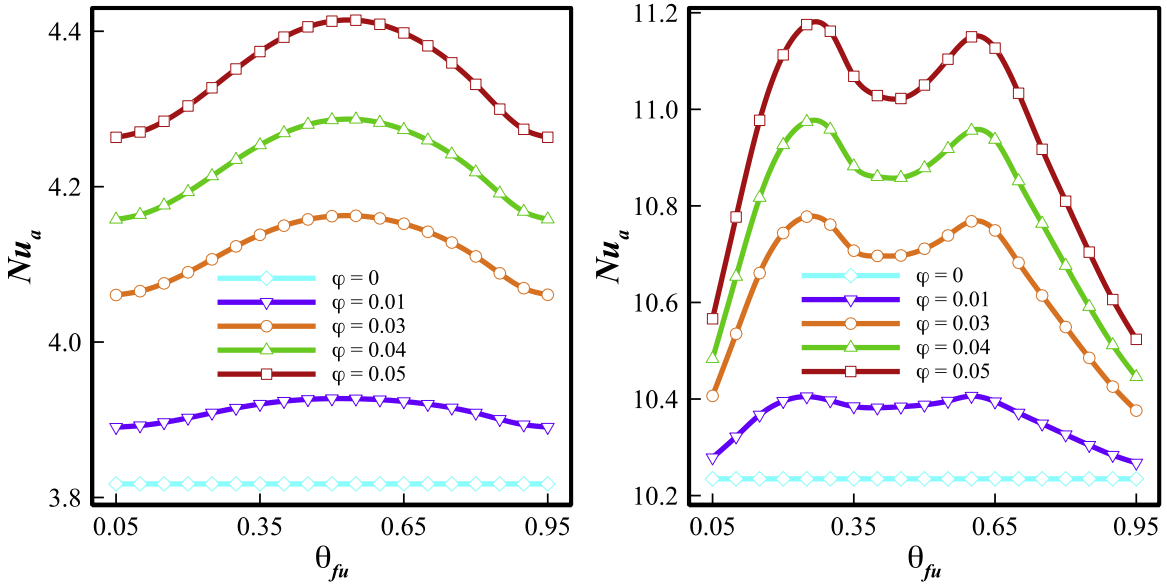

Fig. 9. Variation of the average Nusselt number with θ_{fu} and φ (Da = 0.01, ε = 0.3, E_c= -0.67, and R_r= 2.5): Ra = 10^4 (left) and Ra = 10^6 (right).

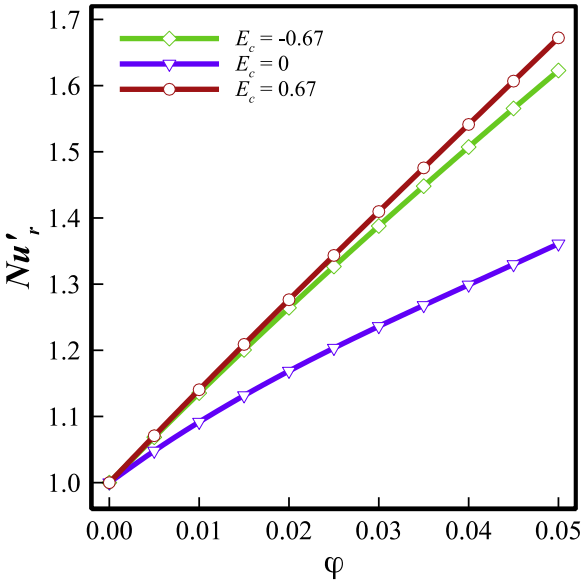

Fig. 10. Variation of the Nu_r' with φ and the eccentricity of the annulus (Ra=10^4, Da=0.1, ε = 0.9, θ_{fu}=0.1, Ste = 0.2 and R_r=2.5).

the highest Nusselt number for the case of Ra = 10^6 can be attributed to its high nonlinearity behaviour of the flow and thermal fields.

To study the influence of the presence of the NEPCMs more precisely, the parameters Nu_r' and Nu_r'' are introduced and described in Section 2.3. Figs. 10 and 11 depict the effect of the nanoparticles' volume fraction on these parameters. Shown in Fig. 10, the Nu_r' increases significantly with the addition nanoparticles. In fact, adding the nano-sized particles to the base fluid, according to the Eqs. (15)-(17), alters the thermo-physical properties of the suspension. The increase of the thermal conductivity of the suspension elevates the rate of conduction heat transfer, and the increment of the viscosity reduces the rate of advection in the annulus. The result reveals that, even with ignoring the latent heat of the cores, the heat transfer intensifies. Moreover, and as previously discussed, the rate of heat transfer increases when the centre of the inner cylinder is located in the lower part of the annulus, i.e. the negative values of the eccentricity.

Fig. 11 outlines the effect of the Stefan number and nanoparticles concentration on the Nu_r'' (normalized Nusselt number with respect to the case of infinite Stefan number) for two values of the fusion temperature (θ_{fu}=0.1 and 0.5). It is worth noting that the Stefan number represents the reciprocal of the latent heat, and thus, the nano-capsules of the PCM behave as simple nanoparticles (without their absorbing/releasing heat mechanisms) as $Ste \to \infty$. Moreover, a Stefan number of 50 is considered to approximate the case of $Ste \to \infty$. Evidently, the Nu_r'' increases slightly with the addition of concentration, indicating that the rate of heat transfer increases when the absorbing/storing/releasing the latent heat of the NEPCMs is enabled. In other words, the rate of transferred heat intensifies when the sole impact of the latent heat of the nano-particles is taken into consideration. Fig. 11 shows that the rate of heat transfer is enhanced more strongly when the fusion temperature of the NEPCMs is around its optimum point (θ_{fu}=0.5 for Ra =10^4, as shown in Fig. 9). More precisely, in comparison with the case of θ_{fu}=0.1, appropriate fusion temperature of the nano-capsules can elevate the rate of heat transfer up to 4% (For example, for φ = 0.05 and Ste = 0.2, $Nu_r'' \approx 1.01$ for θ_{fu}=0.1 and $Nu_r'' \approx 1.05$ for θ_{fu}=0.5). Furthermore, the increasing rate of heat transfer is proportional to the Stefan number, as it is a measure of the non-sensible heat of the NEPCMs.

The dependency of the defined Nusselt numbers on the investigated parameters is shown in Table 4 for a different combination of these parameters. It is evident that the dynamic viscosity number (Nv) and conduction number (Nc) of the NEPCM particles can affect the rate of heat transfer. Nc improves thermal conductivity and Nv aguments the dynamic viscosity for a fixed volume fraction of nanoparticles. As Nv suppressed the convection flow by increasing viscous forces, the heat transfer will be reduced for high Nv. On the other hand, Nc improves the heat transfer rate. As such, for low values of these parameters (first and second rows), presence of the nanoparticles (ignoring their latent heat) reduces the rate of heat transfer ($Nu_r' < 1.0$). It is worth noting that the Nc and Nv about 3.0 could show the typical Maxwell and Brinkman models for thermal conductivity and dynamic viscosity. Moreover, adding nano-capsules of phase change substances always enhance the rate of heat transfer as the Nu_r'' for all of the investigated parameters is above unity, specifying that the rate of heat transfer always in-

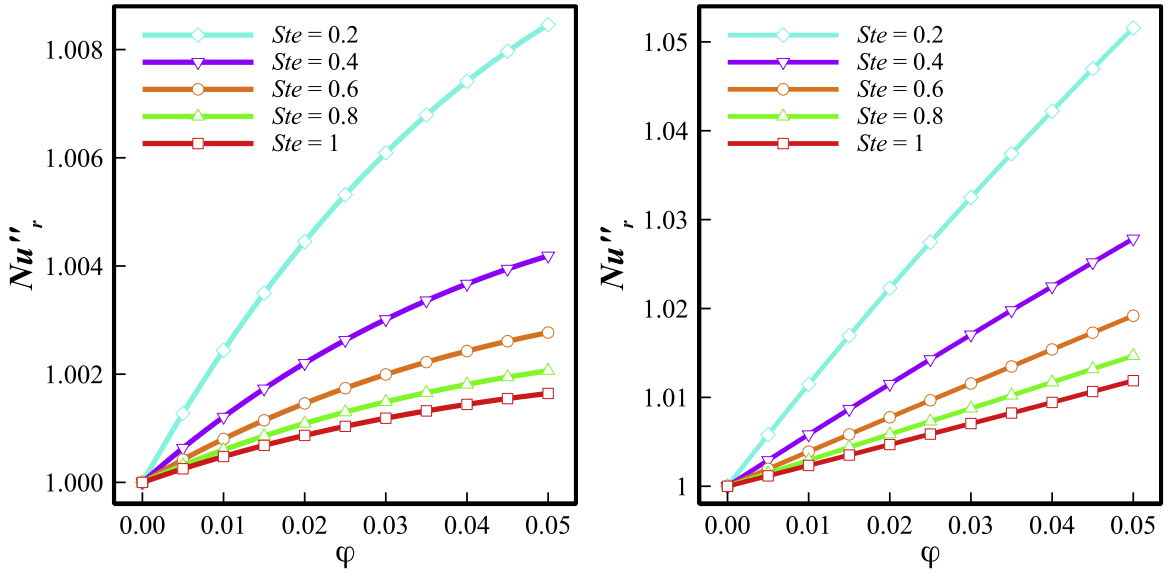

Fig. 11. Variation of the Nu_r'' with the nanoparticles' volume fraction and the Stefan number (Ra=10^4, Da=0.1, ε=0.9, E_c= -0.67 and R_r=2.5): θ_{fu}=0.1 (left) and θ_{fu}=0.5 (right).

Table 4
Influence of the investigated parameters on the defined Nusselt numbers (Da = 0.1, ε = Ste = 0.3).

Ra	Ec	R_r	φ	θ_{fu}	Nc	Nv	Nu_a	Nu_r'	Nu_r''
10^4	0.00	2.5	0.04	0.5	3.0	3.0	3.1055	0.9811	1.0561
10^4	0.00	2.5	0.04	0.5	6.0	12.5	2.9573	0.9443	1.0448
10^4	0.00	2.5	0.00	–	–	–	2.9973	1	1
10^4	-0.67	1.67	0.04	0.1	23.8	12.5	3.5469	1.1015	1.0012
10^4	-0.67	1.67	0.04	0.0	23.8	12.5	3.5426	1.1015	1.0001
10^4	-0.67	1.67	0.04	0.5	23.8	12.5	3.5796	1.1016	1.0104
10^4	-0.67	1.67	0.00	–	–	–	3.2161	1	1
10^4	-0.67	2.5	0.04	0.5	23.8	12.5	4.7225	1.0885	1.0289
10^4	0.00	2.5	0.04	0.5	23.8	12.5	3.2788	1.0526	1.0393
10^4	0.67	2.5	0.04	0.5	23.8	12.5	4.2227	1.1245	1.0186
10^6	-0.67	2.5	0.04	0.5	23.8	12.5	11.3434	1.1703	1.0462
10^6	0.67	2.5	0.04	0.5	23.8	12.5	9.3899	1.0269	1.0525

creases when the latent heat of the NEPCMs is involved. Further, it can be seen that the $Nu_r'' \approx 1.000$ when the fusion temperature is very low (or high, according to Fig. 9). Finally, the Rayleigh number elevates the Nu_a as it intensifies the convection mode of heat transfer.

Fig. 12 shows the influence of the porosity of the solid matrix and the Darcy number on the rate of heat transfer. The Darcy number is, in fact, the non-dimensional permeability of porous medium and characterizes the porous medium resistance to the fluid motion. An increment of the Darcy number, therefore, increases the fluid flow and thus intensifies the convection heat transfer in the annulus. Increasing the porosity of the solid matrix increases the amount of the void space, and hence, more liquid could be filled inside the pores. As a result, the circulation of the suspension could transfer a larger amount of heat by the liquid, which leads to the intensification if the convection heat transfer. On the other hand, the effective thermal conductivity of the solid matrix reduces when ε rises, and thus, the conduction mechanism of the heat transfer declines. As such, for low values of the Darcy number, where the convection heat transfer is poor, the average Nusselt number increases very slightly. Nonetheless, the figure for higher Darcy number is more affected by the porosity of the solid matrix since the convection mode of heat transfer is completely dominant.

Fig. 13 illustrates the influence of the Eccentricity of the inner cylinder and the radii ratio on the rate of heat transfer. As seen, the highest rate of heat transfer can be achieved when the in-

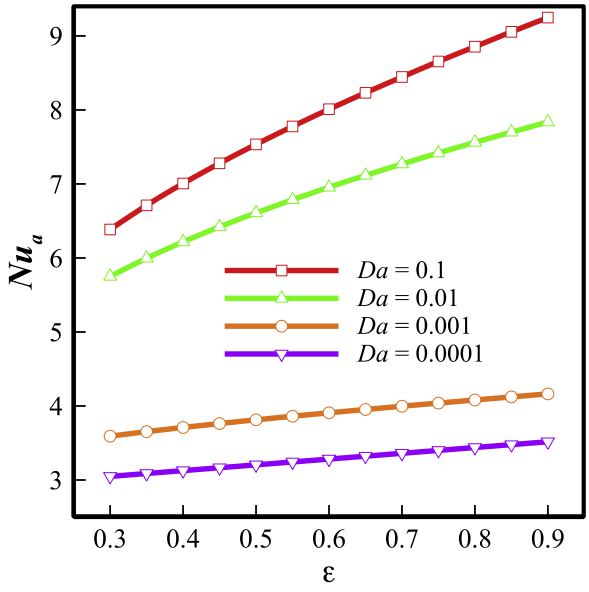

Fig. 12. The average Nusselt number at various Darcy numbers and the porosities (Ra =10^5, φ=0.05, Ste=0.2, θ_{fu}=0.2, E_c=0 and R_r=2.5).

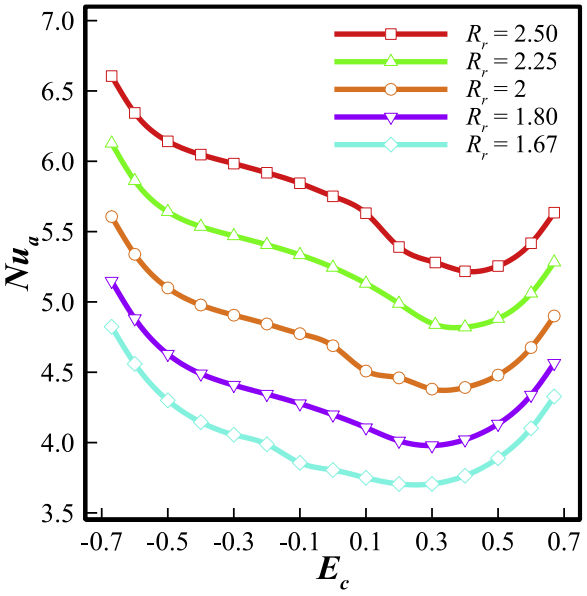

Fig. 13. The average Nusselt number dependency of the suspension to the radii ratio and the eccentricity of the annulus (Ra=10^5, Da=0.01, φ=0.05, Ste = 0.2, θ_{fu}=0.2 and ε = 0.3).

ner cylinder is located in the lower portion of the annulus. As the inner cylinder moves up, the average Nusselt number declines in the annulus (-0.6 $\leq E_c \leq$ 0.4) and then elevates (0.4 $\leq E_c \leq$ 0.6). By increasing the eccentricity, the hot cylinder moves to the area with higher average temperature, and this diminishes the buoyancy force. Therefore, the fluid flow in the annulus reduces (See Fig. 7), resulting in the decline of the convection mode of heat transfer. Nonetheless, when the hot cylinder is positioned adjacent to its cold counterpart, the conduction heat transfer intensifies since the conduction resistance reduces. Ultimately, the rate of convection heat transfer declines when the hot cylinder moves up (for all values of the eccentricity, i.e., -0.6 $\leq E_c \leq$ 0.6).

However, when 0.4 $\leq E_c \leq$ 0.6, the rate of heat transfer augments as its conduction share increases. Besides, the average Nusselt number intensifies as the radii ratio increases. It is worth noting that, as previously shown in Fig. 6, the fluid flow and the rate of heat transfer augment when the radii ratio decreases, and this is attributed to the increment of the hot surface. The $Nu_a$is measured as the rate of heat transfer over the surface of the hot cylinder, and therefore, despite the decline of the heat transfer, the average Nusselt number increases with the increment of the radii ratio.

5. Conclusion

By applying the Galerkin Finite Element Method (FEM), a lattice was formed as a non-uniform structured grid to study the thermal and hydrodynamic behaviour of natural convection in a suspension containing nano-encapsulated phase change materials (NEPCM) in a porous annulus. The inner and outer cylinders were isothermally heated at T_h and T_c, respectively. The suspension was assumed to be diluted, and thus, the homogenous model was acceptable and utilized to address the presence of the nano-sized particle in the base fluid. The phase transition of the phase change materials was modelled as a rise in the heat capacity of the suspension. Influence of key parameters on the flow and thermal fields of the suspension and the rate of heat transfer was analyzed, and the outcomes could be summarized as follows:

1 The average Nusselt number intensifies as the Rayleigh number increases. Moreover, for low values of the Rayleigh number (Ra = 10^6), the rate of heat transfer approaches its maximum when the fusion temperature of the capsule is about 0.5. However, for high Rayleigh numbers (Ra = 10^6), the highest rate of heat transfer can be achieved when the fusion temperature varies between 0.25 $\leq \theta_{fu} \leq$ 0.65.
2 Stefan number represents the reciprocal of the latent heat of the PCM, and thus, the rate of heat transfer intensifies as the Stefan number declines. In other words, the rate of transferred heat increases when the sole impact of the latent heat of the nano-particles is taken into consideration. Further, the rate of heat transfer can be elevated up to 4% when the fusion temperature of the nano-capsules is around $(T_h + T_c)/2$.
3 The heat transfer rate is intensified by adding the nano-capsules with very high Stefan numbers. These specify that the average Nusselt number increases even when the latent heat of the cores of the nano-capsules are ignorable.
4 Moving the cylinder upward first reduces (-0.6 $\leq E_c \leq$ 0.4) and then increases (0.4 $\leq E_c \leq$ 0.6) the average Nusselt number.
5 Increasing the porosity of the solid matrix diminishes the resistance against the flow of the suspension, and thus, the convection heat transfer intensifies. Moreover, the fluid flow increases when the Darcy number rises.
6 When the R_r increases, the fluid flow enhances, and subsequently,the rate of heat transfer declines. However, the average Nusselt number intensifies with the increment of the radii ratio due to the increment of the hot surface of the inner cylinder.

Declaration of Competing Interest

The authors declare that there is no conflict of interest.

Supplementary materials

Supplementary material associated with this article can be found, in the online version, at doi:10.1016/j.ijheatmasstransfer.2020.119792.

References

[1] S.U. Choi, J.A. Eastman, Enhancing thermal conductivity of fluids with nanoparticles, Argonne National Lab., IL (United States), 1995.
[2] K. Khanafer, K. Vafai, M. Lightstone, Buoyancy-driven heat transfer enhancement in a two-dimensional enclosure utilizing nanofluids, Int. J. Heat Mass Transf. 46 (19) (2003) 3639–3653.
[3] S.K. Das, S.U. Choi, W. Yu, T. Pradeep, Nanofluids: science and technology, John Wiley & Sons, 2007.
[4] A. Shenoy, M. Sheremet, I. Pop, Convective flow and heat transfer from wavy surfaces: viscous fluids, porous media, and nanofluids, CRC Press, 2016.
[5] D.A. Nield, A. Bejan, Convection in porous media, Springer, 2006.
[6] O. Mahian, L. Kolsi, M. Amani, P. Estellé, G. Ahmadi, C. Kleinstreuer, J.S. Marshall, M. Siavashi, R.A. Taylor, H. Niazmand, in: Recent advances in modeling and simulation of nanofluid flows-Part I: Fundamentals and theory, 790, Physics reports, 2019, pp. 1–48.
[7] O.Mahian, L.Kolsi, M.Amani, P.Estellé, G.Ahmadi, C.Kleinstreuer, J.S.Marshall, R.A.Taylor, E.Abu-Nada, S.Rashidi, H.Niazmand, Recent advances in modeling and simulation of nanofluid flows–Part II: Applications
[8] N.S. Bondareva, M.A. Sheremet, Conjugate heat transfer in the PCM-based heat storage system with finned copper profile: Application in electronics cooling, Int. J. Heat Mass Transf. 124 (2018) 1275–1284.
[9] N.S. Bondareva, M.A. Sheremet, Flow and heat transfer evolution of PCM due to natural convection melting in a square cavity with a local heater, Int. J. Mech. Sci. 134 (2017) 610–619.
[10] N.S. Bondareva, B. Buonomo, O. Manca, M.A. Sheremet, Heat transfer performance of the finned nano-enhanced phase change material system under the inclination influence, Int. J. Heat Mass Transf. 135 (2019) 1063–1072.
[11] N.S. Bondareva, B. Buonomo, O. Manca, M.A. Sheremet, Heat transfer inside cooling system based on phase change material with alumina nanoparticles, Appl. Therm. Eng. 144 (2018) 972–981.
[12] T. Tayebi, A.J. Chamkha, M. Djezzar, Natural convection of CNT-water nanofluid in an annular space between confocal elliptic cylinders with constant heat flux on inner wall, Scientia Iranica 26 (5) (2019) 2770–2783.
[13] T. Tayebi, A.J. Chamkha, M. Djezzar, Natural convection of CNT-water nanofluid in an annular space between confocal elliptic cylinders with constant heat flux on inner wall, Scientia Iranica. Trans. B Mech. Eng. 26 (5) (2019) 2770–2783.

[14] A.I. Alsabery, M.A. Ismael, A.J. Chamkha, I. Hashim, Effect of nonhomogeneous nanofluid model on transient natural convection in a non-Darcy porous cavity containing an inner solid body, Int. Commun. Heat Mass Transf. 110 (2020) 104442.
[15] A.I. Alsabery, E. Gedik, A.J. Chamkha, I. Hashim, Impacts of heated rotating inner cylinder and two-phase nanofluid model on entropy generation and mixed convection in a square cavity, Heat Mass Transf. 56 (1) (2020) 321–338.
[16] A.I. Alsabery, R. Mohebbi, A.J. Chamkha, I. Hashim, Effect of local thermal non-equilibrium model on natural convection in a nanofluid-filled wavy-walled porous cavity containing inner solid cylinder, Chem. Eng. Sci. 201 (2019) 247–263.
[17] A.I. Alsabery, T. Armaghani, A.J. Chamkha, I. Hashim, Two-phase nanofluid model and magnetic field effects on mixed convection in a lid-driven cavity containing heated triangular wall, Alexandria Eng. J. (2019).
[18] A. Rashad, T. Armaghani, A.J. Chamkha, M. Mansour, Entropy generation and MHD natural convection of a nanofluid in an inclined square porous cavity: effects of a heat sink and source size and location, Chinese J. Phys. 56 (1) (2018) 193–211.
[19] M.S. Ishak, A.I. Alsabery, A. Chamkha, I. Hashim, Effect of finite wall thickness on entropy generation and natural convection in a nanofluid-filled partially heated square cavity, Int. J. Numer. Methods Heat Fluid Flow (2019).
[20] T. Tayebi, A.J. Chamkha, Entropy generation analysis during MHD natural convection flow of hybrid nanofluid in a square cavity containing a corrugated conducting block, Int. J. Numer. Methods Heat Fluid Flow (2019).
[21] A. Alsabery, R. Mohebbi, A. Chamkha, I. Hashim, Impacts of magnetic field and non-homogeneous nanofluid model on convective heat transfer and entropy generation in a cavity with heated trapezoidal body, J. Therm. Anal. Calorimetry 138 (2) (2019) 1371–1394.
[22] A. Arshad, M. Jabbal, P.T. Sardari, M.A. Bashir, H. Faraji, Y. Yan, Transient simulation of finned heat sinks embedded with PCM for electronics cooling, Therm. Sci. Eng. Progress (2020) 100520.
[23] A. Chamkha, A. Doostanidezfuli, E. Izadpanahi, M. Ghalambaz, Phase-change heat transfer of single/hybrid nanoparticles-enhanced phase-change materials over a heated horizontal cylinder confined in a square cavity, Adv. Powder Tech. 28 (2) (2017) 385–397.
[24] P.T. Sardari, D. Giddings, D. Grant, M. Gillott, G.S. Walker, Discharge of a composite metal foam/phase change material to air heat exchanger for a domestic thermal storage unit, Renew. Energy 148 (2020) 987–1001.
[25] P.T. Sardari, D. Grant, D. Giddings, G.S. Walker, M. Gillott, Composite metal foam/PCM energy store design for dwelling space air heating, Energy Convers. Manage. 201 (2019) 112151.
[26] Z. Li, A. Shahsavar, A.A. Al-Rashed, P. Talebizadehsardari, Effect of porous medium and nanoparticles presences in a counter-current triple-tube composite porous/nano-PCM system, Appl. Therm. Eng. 167 (2020) 114777.
[27] S. Barlak, O.N. Sara, A. Karaipekli, S. Yapıcı, Thermal conductivity and viscosity of nanofluids having nanoencapsulated phase change material, Nanoscale Microscale Thermophys. Eng. 20 (2) (2016) 85–96.
[28] Y. Zhu, Y. Qin, C. Wei, S. Liang, X. Luo, J. Wang, L. Zhang, Nanoencapsulated phase change materials with polymer-SiO2 hybrid shell materials: Compositions, morphologies, and properties, Energy Convers. Manage. 164 (2018) 83–92.
[29] A. Zhao, J. An, J. Yang, E.-H. Yang, Microencapsulated phase change materials with composite titania-polyurea (TiO2-PUA) shell, Appl. Energy 215 (2018) 468–478.
[30] Y. Zhu, Y. Chi, S. Liang, X. Luo, K. Chen, C. Tian, J. Wang, L. Zhang, Novel metal coated nanoencapsulated phase change materials with high thermal conductivity for thermal energy storage, Solar Energy Mater. Solar Cells 176 (2018) 212–221.
[31] N. Navarrete, R. Mondragón, D. Wen, M.E. Navarro, Y. Ding, J.E. Juliá, Thermal energy storage of molten salt–based nanofluid containing nano-encapsulated metal alloy phase change materials, Energy 167 (2019) 912–920.
[32] X. Du, Y. Fang, X. Cheng, Z. Du, M. Zhou, H. Wang, Fabrication and characterization of flame-retardant nanoencapsulated n-octadecane with melamine—formaldehyde shell for thermal energy storage, ACS Sustain. Chem. Eng. 6 (11) (2018) 15541–15549.
[33] H.R. Seyf, Z. Zhou, H. Ma, Y. Zhang, Three dimensional numerical study of heat-transfer enhancement by nano-encapsulated phase change material slurry in microtube heat sinks with tangential impingement, Int. J. Heat Mass Transf. 56 (1–2) (2013) 561–573.
[34] H. Reza Seyf, M.R. Wilson, Y. Zhang, H. Ma, Flow and heat transfer of nanoencapsulated phase change material slurry past a unconfined square cylinder, J. Heat Transf. 136 (5) (2014).
[35] C.-J. Ho, W.-C. Chen, W.-M. Yan, Experimental study on cooling performance of minichannel heat sink using water-based MEPCM particles, Int. Commun. Heat Mass Transf. 48 (2013) 67–72.
[36] C.-J. Ho, J. Huang, P. Tsai, Y.M. Yang, Water-based suspensions of Al2O3 nanoparticles and MEPCM particles on convection effectiveness in a circular tube, Int. J. Therm. Sci. 50 (5) (2011) 736–748.
[37] C.-J. Ho, W.-C. Chen, W.-M. Yan, Correlations of heat transfer effectiveness in a minichannel heat sink with water-based suspensions of Al2O3 nanoparticles and/or MEPCM particles, Int. J. Heat Mass Transf. 69 (2014) 293–299.
[38] M. Eisapour, A.H. Eisapour, M. Hosseini, P. Talebizadehsardari, Exergy and energy analysis of wavy tubes photovoltaic-thermal systems using microencapsulated PCM nano-slurry coolant fluid, Appl. Energy 266 (2020) 114849.
[39] M. Ghalambaz, A.J. Chamkha, D. Wen, Natural convective flow and heat transfer of nano-encapsulated phase change materials (NEPCMs) in a cavity, Int. J. Heat Mass Transf. 138 (2019) 738–749.
[40] S. Mehryan, M. Ghalambaz, L.S. Gargari, A. Hajjar, M. Sheremet, Natural convection flow of a suspension containing nano-encapsulated phase change particles in an eccentric annulus, J. Energy Storage 28 (2020) 101236.
[41] A. Hajjar, S. Mehryan, M. Ghalambaz, Time periodic natural convection heat transfer in a nano-encapsulated phase-change suspension, Int. J. Mech. Sci. 166 (2020) 105243.
[42] M. Ghalambaz, T. Groşan, I. Pop, Mixed convection boundary layer flow and heat transfer over a vertical plate embedded in a porous medium filled with a suspension of nano-encapsulated phase change materials, J. Mol. Liquids 293 (2019) 111432.
[43] M.Ghalambaz, S.Mehryan, A.Hajjar, A.Veisimoradi, Unsteady natural convection flow of a suspension comprising Nano-Encapsulated Phase Change Materials (NEPCMs) in a porous medium, Advanced Powder Technology, (2019).
[44] L. Chai, R. Shaukat, L. Wang, H.S. Wang, A review on heat transfer and hydrodynamic characteristics of nano/microencapsulated phase change slurry (N/MPCS) in mini/microchannel heat sinks, Appl. Therm. Eng. 135 (2018) 334–349.
[45] K. Khanafer, K. Vafai, A critical synthesis of thermophysical characteristics of nanofluids, Int. J. Heat Mass Transf. 54 (19–20) (2011) 4410–4428.
[46] B. Chen, X. Wang, R. Zeng, Y. Zhang, X. Wang, J. Niu, Y. Li, H. Di, An experimental study of convective heat transfer with microencapsulated phase change material suspension: laminar flow in a circular tube under constant heat flux, Exp. Therm. Fluid Sci. 32 (8) (2008) 1638–1646.
[47] A. Zaraki, M. Ghalambaz, A.J. Chamkha, M. Ghalambaz, D. De Rossi, Theoretical analysis of natural convection boundary layer heat and mass transfer of nanofluids: effects of size, shape and type of nanoparticles, type of base fluid and working temperature, Adv. Powder Tech. 26 (3) (2015) 935–946.
[48] T. Kuehn, R. Goldstein, An experimental and theoretical study of natural convection in the annulus between horizontal concentric cylinders, J. Fluid Mech. 74 (4) (1976) 695–719.
[49] M.H. Matin, I. Pop, Natural convection flow and heat transfer in an eccentric annulus filled by Copper nanofluid, Int. J. Heat Mass Transf. 61 (2013) 353–364.
[50] P. Nithiarasu, K. Seetharamu, T. Sundararajan, Natural convective heat transfer in a fluid saturated variable porosity medium, Int. J. Heat Mass Transf. 40 (16) (1997) 3955–3967.